Deterministic quantities characterizing noise driven Hopf bifurcations in gas turbine combustors

Nicolas Noiray, Bruno Schuermans

Alstom Power, Baden, Switzerland

Abstract

Lean premix gas turbine combustors are prone to high amplitude pressure oscillations driven by nonlinear thermoacoustic coupling. These pulsations are unwanted because they can affect the lifetime of the combustor parts. The standard strategy to get rid of these oscillations is to implement acoustic damping devices. Knowing the deterministic components characterizing the acoustic-flame coupling, the linear growth rates in particular, is necessary to properly design the dampers. However, the time scale associated with the variations of the engine operating conditions are much larger than the one of the acoustic pressure amplitude dynamics. Therefore, the linearly unstable system cannot be observed during the exponential amplitude growth of one of the acoustic eigenmodes and it is not possible to directly determine the linear growth rates. They can only be estimated from signals recorded when the system is operating on limit cycling states. Fortunately, these states are driven by a strong stochastic forcing produced by the highly turbulent reactive flow. It is shown in this article that the deterministic quantities can be extracted from the noise perturbed limit cycles data by making use of the stochastic differential equations describing the combustion instabilities. A straightforward experimental set-up allowing to reproduce the main features of the thermoacoustic coupling observed in gas turbines is used to validate the proposed identification methods. In a second step, these latter methods are applied to engine data.

Keywords: Thermoacoustics; Combustion instabilities; Gas turbine; Stochastic Hopf bifurcation; Van der Pol oscillator.

1. Introduction

Getting rid of combustion instabilities is one of the strenuous challenges that engineers developing gas turbine combustion chambers must meet. Constructive interaction between flames and combustor acoustic eigenmodes can yield large amplitude pressure oscillations which induce vibrations and in turn decrease the lifetime of the structural part. This phenomenon has been studied for a long time and one can find an interesting collection of paper dealing with that subject in [1]. Nevertheless, the plurality of acoustic eigenmodes which can nonlinearly couple with the flames

This is a pre-print version. Published in *International Journal of Non-Linear Mechanics* (2013) Vol. 50, p. 152-163, DOI: 10.1016/j.ijnonlinmec.2012.11.008

and the progressively more stringent emission regulations for NOx, CO and unburned hydrocarbon keep the researchers busy with that topic in order to increase the operational flexibility of the engines.

Significant progress were recently made in terms of thermoacoustic coupling modeling and were reported in numerous studies. Among these, the nonlinear features of flame dynamics were investigated through the describing function methodology [2, 3, 4, 5, 6] and a theoretical framework accounting for non-normal interactions between thermoacoustic eigenmodes has been introduced to model transient energy growths which might be a possible explanation for triggering of oscillating states pertaining to stable branch of sub-critical Hopf bifurcations e.g. [7, 8].

An efficient way of preventing combustion instabilities is to implement dampers in the combustor in order to increase the acoustic dissipation of the system. The knowledge of the linear growth rates associated to the thermoacoustic coupling enables to properly design these dampers as shown in [9] and avoid any over or under estimation of their volume. This is important due to the fact that space for damping equipment is generally limited.

The difficulty lies in the fact that when the origin is asymptotically unstable, the system is always observed on a limit cycling state, which in turn prevents from directly estimating growth rates by considering the exponential growth of the oscillation amplitude from the origin. This is because the time taken to change the gas turbine operating conditions to cross the Hopf bifurcation is much longer than the characteristic time of the acoustic amplitude dynamics.

In the early 90s, active control has been used to observe the growth of initially small perturbations and to measure linear growth rate [10]. More recently [3], the flame describing function approach was used to predict linear growth rates and limit cycle amplitudes. However, such strategies do only apply to laboratory facilities and test rigs equipped with excitation systems powerful enough to drive the oscillation at a level where the flames non-linearly interact with the acoustic waves. Moreover, the aim in [3] is to *predict* the deterministic properties of the system – in particular the linear growth rate – by using the knowledge of the dynamics of the subsystems considered independently – i.e. the flame response and the acoustic propagation within the combustor – whereas in the present study, the objective is to *extract* these deterministic quantities by observing the system as a whole.

Without active control device, the state of the art in estimating deterministic quantities characterizing thermoacoustic coupling in combustion chambers from dynamic pressure time series is limited to the case of linearly stable conditions. One can for example refer to the work reported in [11, 12, 13]. As stressed by Culick in the chapter 7-10 of his monograph [14], the methods presented in these references provide the stability margin associated to a given operating condition, i.e. the damping rate, but they do not apply to an asymptotically unstable regime for which the amplitude is limited by nonlinear mechanisms and they cannot be used to extract the corresponding linear growth rate.

In this paper, we show that it is possible to measure this latter quantity by making use of the intense background noise generated by the highly turbulent reactive flow in the combustion chamber. This

This is a pre-print version. Published in *International Journal of Non-Linear Mechanics* (2013) Vol. 50, p. 152-163, DOI: 10.1016/j.ijnonlinmec.2012.11.008

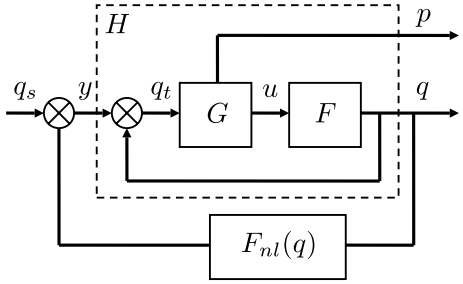

Figure 1: Block diagram of a generalized thermo acoustic system with stochastic heat release source term q_s as input, and measured pressure fluctuations p as output. All linear (thermo–) acoustic interactions are contained in H, the non-linear part of the system is contained in F_{nl}. The transfer function G represents the passive acoustic dynamics, F represents the flame transfer function.

inherent stochastic forcing is a major driver of the limit cycle dynamics but its influence is barely documented and most of the investigations dealing with thermoacoustic coupling are restricted to deterministic stability analysis. There is a small number of studies in which the background noise impact on combustion instabilities as been described and analyzed: theoretical and experimental material giving *qualitative* insight into the influence of this noise on limit cycles were presented in [15, 16, 17] or recently in [18]. It is shown in the present paper that *quantitative* estimation of the growth rates can also be obtained by furthering the analysis of the stochastic differential equations introduced in the aforementioned references.

The parameters identification approaches derived in the following section are based on the equations governing stochastically driven oscillators with nonlinear damping. The corresponding foundations were settled decades ago and one can for instance refer to the major contribution from Stratonovich [19] or to the subsequent outstanding papers [20] or [21]. The growth rate identification approaches are then validated using a noise driven electroacoustic Van der Pol oscillator which mimic the thermoacoustic coupling operating in combustion chambers. In the last part, they are applied to engine data.

2. Theoretical model

2.1. Thermo-acoustic coupling in combustion chambers

A thermoacoustic system can conceptually be represented by a block diagram (e.g. [22]). In the present work, one considers the one depicted in figure 1. In this system, the heat release fluctuations by the combustion process, q_t, act as a source term for the acoustic field. Wave propagation through the various components of the combustion system, including reflection and damping on the boundaries and at area discontinuities is represented by the system G. It will be assumed here that these wave propagation phenomena are linear. The response of the flame to an acoustic perturbation can be assumed to be linear for small amplitude perturbations, however for

This is a pre-print version. Published in *International Journal of Non-Linear Mechanics* (2013) Vol. 50, p. 152-163, DOI: 10.1016/j.ijnonlinmec.2012.11.008

sufficiently large amplitudes this assumption will no longer hold. Nevertheless, the flame response can conceptually be split in a linear part and a non–linear part. The linear response of the flame to acoustic velocity perturbations u is described by a transfer function F[1]. The linear heat release response is denoted as q, the sum of the purely non-linear part and the stochastic part of the heat release is denoted by y. All non-linear processes are contained in the function $F_{nl}(q)$. By definition, F_{nl} will not contain any linear parts, i.e., $\lim_{q\to 0} dF_{nl}(q)/dq = 0$. It might seem physically more correct to express the flame nonlinearity as a function of u rather than q, however it is clear that mathematically this doesn't matter because q is a linear function of u. As pointed out by a reviewer, equivalence ratio fluctuations – which do not appear explicitly in figure 1 – are significantly contributing to the flame response when practical fuel injection systems are used. According to [23, 24, 25], these equivalence ratio fluctuations are linearly and non-linearly linked to the acoustic perturbations. One can therefore consider that their influence is comprised in F and F_{nl}.

The part of the heat release that has a stochastic nature (typically due to turbulent combustion noise) is denoted as q_s which is the input to the system. Thus, the heat release fluctuations are considered to be a superposition of three contributions: a stochastic part, a part that depends linearly on the acoustic field and a part that depends non-linearly on the acoustic field. The signal p represents the measurement of the acoustic pressure fluctuations at one or more locations.

By collecting all linear elements in one system H, the system can be described by a feedback interconnection of a linear system with a purely non-linear system:

$$\begin{aligned} \begin{bmatrix} q \\ p \end{bmatrix} &= H(s)\, y \\ y &= F_{nl}(q) + q_s \end{aligned} \tag{1}$$

Although the linear transfer functions G and F are typically stable (i.e. they have eigenvalues with negative real parts), the system H can be unstable due to the feedback of the heat release q. It can be shown via a similarity transform[2] based on the systems eigenvectors that any linear non-degenerate system H can be represented by the following state–space system:

$$\frac{\partial}{\partial t}\begin{bmatrix} \boldsymbol{\eta} \\ \dot{\boldsymbol{\eta}} \\ \mathbf{x} \end{bmatrix} = \underbrace{\begin{bmatrix} \mathbf{0} & \mathbf{I} & \mathbf{0} \\ -\boldsymbol{\Omega}^{\mathbf{2}} & 2\,\boldsymbol{\nu} & \mathbf{0} \\ \mathbf{0} & \mathbf{0} & \boldsymbol{\lambda}_{\mathbf{r}} \end{bmatrix}}_{\mathbf{A}} \begin{bmatrix} \boldsymbol{\eta} \\ \dot{\boldsymbol{\eta}} \\ \mathbf{x} \end{bmatrix} + \begin{bmatrix} \mathbf{0} \\ \mathbf{B} \\ \mathbf{B}_{\mathbf{r}} \end{bmatrix} y \tag{2}$$

$$\begin{bmatrix} q \\ p \end{bmatrix} = \mathbf{C}\begin{bmatrix} \boldsymbol{\eta} \\ \dot{\boldsymbol{\eta}} \\ \mathbf{x} \end{bmatrix} + \mathbf{D}\, y\,, \tag{3}$$

[1]The flame can also respond to acoustic pressure fluctuations, the treatment is completely analogous but for simplicity of notation only coupling via acoustic velocity will be considered here.

[2]Note that the similarity transform does not change the input-output relation of the system, nor its eigenvalues

This is a pre-print version. Published in *International Journal of Non-Linear Mechanics* (2013) Vol. 50, p. 152-163, DOI: 10.1016/j.ijnonlinmec.2012.11.008

In which, $\mathbf{\Omega^2}$ is a diagonal matrix containing the squared absolute values of the complex eigenvalues ($\lambda_n = \nu_n \pm i\,\omega_n$) of the system, $\boldsymbol{\nu}$ is a diagonal matrix containing the real part of the complex eigenvalues, $\mathbf{I}$ is the unity matrix and $\boldsymbol{\lambda}_\mathbf{r}$ is a diagonal matrix containing the real-valued eigenvalues. Because it will take finite time for an acoustic wave to propagate through the system, the direct feedthrough gain $\mathbf{D}$ will be considered zero in the subsequent analysis. The states η_n, $\dot{\eta}_n$ and x in the state vectors $\boldsymbol{\eta}$, $\dot{\boldsymbol{\eta}}$ and $\mathbf{x}_\mathbf{r}$ represent the dynamics of the modes of the system associated with their complex and real eigenvalues. It is worth emphasizing that all pairs $(\eta_n, \dot{\eta}_n)$ are independent of each other, because the similarity transform is chosen such that matrix $\mathbf{A}$ has orthogonal[3] eigenvectors and hence $\mathbf{A}\,\mathbf{A}^T = \mathbf{A}^T\,\mathbf{A}$.

It will be assumed that the nonlinear response $F_{nl}(q)$ is insignificant for sufficiently small amplitudes of q. Hence, the poles or eigenvalues of the system H define the linear stability of the system: if the real part of one of the eigenvalues λ is positive, then the system H is linearly unstable. The pressure distribution associated with each mode is referred to as it's mode shape. Each of the modes oscillates at frequency ω_n, and will have a grow or decay rate ν_n in the linear regime. If the amplitudes q reach sufficiently high levels, the non-linear response cannot be neglected anymore. Limit cycles occur if the nonlinearity is such that it counter-acts the linear amplification and hence renders the non-linear system stable. Even if the system is non-linearly stabilized in this manner, the limit cycle amplitudes will not be constant: the amplitudes will fluctuate in a stochastic manner around a non-zero mean level due to the stochastic driving term q_s. It will be shown that the stochastic properties of these fluctuations of the limit cycle amplitude are related to the linear growth rate of the system.

Depending on the complexity of the system, G will have many eigenvalues, but only a few will be of concern: those with the largest real parts. In practice, the system dynamics is generally governed by one of the eigenmodes at a given operating condition. We therefore limit our analysis to the dynamics related to only one pair $(\eta, \dot{\eta})$ associated to one eigenvalue pair ($\lambda = \nu \pm i\,\omega_0$). It will be assumed that $\nu \ll \omega_0$.

$$\begin{aligned} \ddot{\eta} - 2\nu\,\dot{\eta} + \omega_0^2\,\eta &= b\,y \\ q &= c_{11}\,\eta + c_{12}\,\dot{\eta} \end{aligned} \tag{4}$$

in which b and c_{11} and c_{12} are constant and real valued. Substituting $y = F_{nl}(q) + q_s$ yields:

$$\ddot{\eta} + \omega_0^2\,\eta = 2\nu\,\dot{\eta} + b\,F_{nl}(c_{11}\,\eta + c_{12}\,\dot{\eta}) + b\,q_s \tag{5}$$

It has been shown experimentally in e.g. [3] that the nonlinearity does not only act on the amplitude of oscillation, but can also induce a phase shift, i.e the nonlinearity cannot be considered static but is generally dynamic. However, in vicinity of ω_n a *dynamic* nonlinearity can be represented by a *static* nonlinear function of η and it's time derivative. It is straightforward to show that no

[3]This does not exclude the possibility of so–called non–normal growth of the energy of the system, see the appendix.

This is a pre-print version. Published in *International Journal of Non-Linear Mechanics* (2013) Vol. 50, p. 152-163, DOI: 10.1016/j.ijnonlinmec.2012.11.008

higher order time derivatives or integrals of η are needed because for $\omega = \omega_0$ these will all be linear combinations of η and $\dot{\eta}$. Thus, eq. (5) can be written as:

$$\ddot{\eta} + \omega_0^2 \eta = f(\eta, \dot{\eta}) + \xi, \tag{6}$$

with $\xi = b\, q_s$. In the case of thermo-acoustic coupling occurring in combustion chambers, the process ξ is induced by the turbulent combustion noise. The intensity of this non-coherent forcing follows a power law decay [26]:

$$\frac{\partial P}{\partial \omega} \propto \omega^{-5/2},$$

where P denotes the power spectral density of the radiated noise. One can also refer to the recent studies proposed in [27, 28] providing a good overview of the spectral content of the noise radiated by premixed flames. When the system is evolving on a limit cycle, the peak in the spectrum is usually very sharp compared to the smooth variations of the turbulent combustion noise intensity. As a first approximation, it is assumed that ξ is a stationary, delta-correlated and normally distributed random process with $\langle \xi \xi_\tau \rangle = \Gamma \delta(\tau)$ and that the process η is Markovian. Rigorous substantiation of this assumption is under investigation. Nevertheless, it will be shown in what follows that the results obtained with this idealized forcing term are in very good agreement with the observations.

When the r.h.s. term of eq. (6) is small compared to both terms on the l.h.s., η will be quasi-sinusoidal. It is therefore adequate, to investigate the system in the amplitude-phase coordinate system:

$$A = \sqrt{\eta^2 + (\dot{\eta}/\omega_0)^2} \quad \text{and} \quad \varphi = -\arctan\left(\frac{\dot{\eta}}{\omega_0 \eta}\right) - \omega_0 t, \tag{7}$$

with $\eta = A\cos(\omega_0 t + \varphi) = A\cos\phi$. By differentiating (7) with respect to time, one gets:

$$\dot{A} = -\frac{\sin\phi}{\omega_0}\left[\, f(A\cos\phi, -A\omega_0 \sin\phi) + \xi \,\right] \quad \text{and} \quad \dot{\varphi} = -\frac{\cos\phi}{A\omega_0}\left[\, f(A\cos\phi, -A\omega_0 \sin\phi) + \xi \,\right] \tag{8}$$

The function f is now expanded as a Taylor series:

$$f(\eta, \dot{\eta}) = \sum_n \sum_m \gamma_{n,m}\, \eta^n\, \dot{\eta}^m. \tag{9}$$

Substituting this expansion in eq. (8), and applying deterministic and stochastic averaging (respectively refer to [29] and [19]) yields:

$$\dot{A} = \frac{1}{2}\gamma_{0,1} A + \left(\frac{1}{8}\gamma_{2,1} + \frac{3\omega_0^2}{8}\gamma_{0,3}\right) A^3 + \frac{\Gamma}{4\omega_0^2 A} + \zeta + \mathcal{O}(A^5) \tag{10}$$

$$\dot{\varphi} = -\frac{1}{2}\gamma_{1,0} - \left(\frac{\omega_0}{8}\gamma_{1,2} + \frac{3}{8\omega}\gamma_{3,0}\right) A^2 + \frac{1}{A}\chi + \mathcal{O}(A^5) \tag{11}$$

where χ and ζ are two uncorrelated white noise excitations, each featuring the same noise intensity $\Gamma/2\omega_0^2$. On the one hand, the form of eq. (10) truncated to the third order is the amplitude

This is a pre-print version. Published in *International Journal of Non-Linear Mechanics* (2013) Vol. 50, p. 152-163, DOI: 10.1016/j.ijnonlinmec.2012.11.008

equation of a stochastic Van der Pol oscillator (e.g. [30]). On the other hand it has been observed by the authors that the first two terms in the l.h.s. of eq. (11) have negligible contribution. This conclusion was drawn from the analysis of the random process φ from acoustic data obtained in a gas turbine combustor. Therefore, the general amplitude-phase SDEs (10) and (11) reduce to:

$$\dot{A} = A\left(\frac{\beta-\alpha}{2} - \frac{\kappa}{8}A^2\right) + \frac{\Gamma}{4\omega_0^2 A} + \zeta, \tag{12}$$

$$\dot{\varphi} = \frac{1}{A}\,\chi, \tag{13}$$

where $\gamma_{0,1} = 2\nu$ has been replaced by $\beta - \alpha$. The positive constant α stands for the linear acoustic absorption in the volume and at the boundaries and β for the linear contribution of the feedback induced by the flame which can be either negative or positive. In this latter situation the linear terms are competing and a Hopf bifurcation is crossed at $\alpha = \beta$. In fact, eqs. (12) and (13) are the amplitude and phase equation of a stochastic Van der Pol oscillator with $f(\eta, \dot{\eta}) = \dot{\eta}(\beta - \alpha - \kappa\eta^2)$.

2.2. System identification

At this point, the basic equations that are needed for the extraction of deterministic quantities from acoustic pressure time traces have been settled. Several identification methods are now presented. For linearly stable system, it is possible to apply the approach proposed in section 2.2.1, while the ones presented in 2.2.2 and 2.2.3 can be used for linearly unstable system. The method given in 2.2.4 can be equally applied to linearly stable and unstable systems. The unknown that have to be identified are the oscillator's eigenfrequency ω_0, the linear growth/damping rate[4] $\nu = (\beta - \alpha)/2$, the noise intensity Γ and the nonlinearity coefficient κ which defines the deterministic limit cycle amplitude $A_0 = (8\nu/\kappa)^{1/2}$. Note that since $p = c_{21}A\cos\phi - c_{21}\omega_0 A\sin\phi$, the acoustic pressure amplitude is linearly proportional to A and one can perform these deterministic parameters identification using the pressure signal, provided that the neighboring system's eigenfrequencies are distant.

2.2.1. Power spectral density of the acoustic pressure

The oscillator featuring a negative growth rate, i.e. $\alpha > \beta \Rightarrow \nu < 0$ is first considered. In this situation the system is linearly stable and the equilibrium is the attractor. When this system is driven by stochastic forcing, one can make use of the power spectral density in order to extract ν and Γ. The nonlinear part of the forcing is neglected in the model and one can write eq. (6) in the form:

$$\ddot{\eta} - 2\nu\,\dot{\eta} + \omega_0^2\eta = \xi. \tag{14}$$

[4]Note that in contrast with ref. [3], ν does not depend on the oscillation amplitude. This is because the growth rate considered in the "Flame describing function" framework [3] is the one associated to the system linearized around a given amplitude. Therefore, it implicitly contains the effect of nonlinearity at each particular amplitude; it decreases and ultimately vanishes when approaching the limit cycle. Here, the so-called "linear growth rate" is the real part of the linear system's eigenvalue and it corresponds to the growth rate discussed in the "Flame transfer function" framework.

This is a pre-print version. Published in *International Journal of Non-Linear Mechanics* (2013) Vol. 50, p. 152-163, DOI: 10.1016/j.ijnonlinmec.2012.11.008

One can then write

$$\mathcal{S}_{\eta\eta} = \frac{1}{2\pi} \frac{\Gamma}{(\omega_0^2 - \omega^2)^2 + 4\nu^2\omega^2} \tag{15}$$

The unknown quantities ω_0, ν and Γ can be obtained by fitting eq. (15) on the power spectral density of the measured dynamic pressure. Note that this approach applies only to linearly stable systems and it is not valid when the stochastic driving is so strong that the nonlinear nature of the response cannot be neglected anymore.

2.2.2. Power spectral density of the amplitude fluctuations

The case of a weakly perturbed limit cycle is now considered. The linear growth rate ν is positive and the noise intensity Γ is small enough to allow a linearization of the simplified equations (12) and (13). It is therefore assumed that the limit cycle amplitude fluctuations A' induced by the stochastic forcing are small compared to the deterministic limit cycle amplitude $A_0 = (8\nu/\kappa)^{1/2}$, which is the stationary solution of eq. (12) without stochastic terms. The amplitude is decomposed in a mean and fluctuating components $\bar{A}$ and A', where $A' \ll \bar{A}$. Keeping the first order terms in eq. (12) and considering that $\bar{A} \approx A_0$ since the stochastic forcing is weak, yields

$$\dot{A}' = -\left(2\nu + \frac{\Gamma}{4\omega_0^2 A_0^2}\right) A' \, + \, \zeta. \tag{16}$$

The normalized form of the power spectral density of the amplitude fluctuations is then given by

$$\frac{\mathcal{S}_{A'A'}(\omega)}{\bar{A}^2} \quad = \quad \frac{c_0/\pi}{\omega^2 + (2\nu + c_0)^2} \tag{17}$$

where $c_0 = \Gamma/4\omega_0^2 A_0^2$. It is then possible to extract the linear growth rate ν and the noise intensity Γ by fitting with eq. (17) the power spectral density of the dynamic pressure amplitude, this latter quantity being obtained by applying Hilbert transform to the measured pressure signal. Note that this method is valid only if the Van der Pol limit cycle is weakly perturbed by additive white noise. In such situation where $\nu \gg c_0$, the correlation time of the amplitude's fluctuations is equal to half the inverse of the linear growth rate.

2.2.3. Stationary solution of the Fokker-Planck equation

It is now interesting to consider a more general approach based on the Fokker-Planck equation associated with the amplitude and phase stochastic differential equations. In particular, the applicability range of this method is not restricted to low noise intensity level as it was the case with the linearization method. Eq. (12) has the form of a Langevin equation containing a nonlinear damping term. It can be written as a stochastic differential equation in the Îto sense:

$$dA = \mathcal{F}(A)\, dt + dW \quad \text{where} \quad dW = \zeta\, dt, \tag{18}$$

$$\text{and} \quad \mathcal{F}(A) = A\left(\nu - \frac{\kappa}{8}A^2\right) + \frac{\Gamma}{4\omega_0^2 A} \tag{19}$$

This is a pre-print version. Published in *International Journal of Non-Linear Mechanics* (2013) Vol. 50, p. 152-163, DOI: 10.1016/j.ijnonlinmec.2012.11.008

In this equation, dW is an increment of a Wiener process coming from the Gaussian white noise ζ featuring the intensity $\Gamma/(2\omega_0^2)$. Recall that ζ is assumed to be delta-correlated despite it has a non vanishing correlation time in real applications. This hypothesis holds when the time constant characterizing the variations of the amplitude is much larger than the correlation time of the stochastic forcing. This assumption guarantees that the probability density of the amplitude obeys the following Fokker-Planck equation

$$\frac{\partial}{\partial t}p(A,t) = -\frac{\partial}{\partial A}\left[\mathcal{F}(A)p(A,t)\right] + \frac{\Gamma}{4\omega_0^2}\frac{\partial^2}{\partial A^2}p(A,t) \tag{20}$$

Accounting for the fact that the density is vanishing when the amplitude tends to infinity, one can write that the stationary probability density is solution of

$$\frac{d}{dA}p(A) - \frac{4\omega_0^2}{\Gamma}\mathcal{F}(A)p(A) = 0. \tag{21}$$

It is given by

$$p(A) = \frac{\sqrt{4\nu/\pi c_0}}{A_0^2\ \mathrm{erfc}\left(-\sqrt{\nu/4c_0}\right)} A \exp\left(-\frac{\nu}{c_0}\left(\frac{A^2-A_0^2}{2A_0^2}\right)^2\right) \tag{22}$$

where $A_0 = \sqrt{8\nu/\kappa}$ is the deterministic limit cycle amplitude and $c_0 = \Gamma/4\omega_0^2A_0^2$. Note that the probability density is function of the ratio ν/c_0 which gives the balance between the limit cycle strength characterized by the oscillator's linear growth rate and the normalized stochastic forcing level. An estimate of the ratio ν/c_0 can therefore be obtained together with the deterministic limit cycle amplitude A_0 by fitting the experimentally obtained density function $p(A)$ with eq. (22). Alternatively, the ratio ν/c_0 can be obtained from $p(\eta)$. This latter density function can be deduced from the density $p(A,\varphi)$ of the joint Markov process (A,φ). When stationary state is established, φ is a uniformly distributed process with $p(\varphi) = 1/2\pi$, and one can write $p(A,\varphi) = p(A)p(\varphi) = p(A)/2\pi$, which was shown in [21] and used for instance in [30]. Making use of the fact that $p(A,\varphi) = J_{A,\varphi\to\eta,\dot\eta}\,p(\eta,\dot\eta)$, where J is the Jacobian, one gets $p(A,\varphi) = A\omega_0\ p(\eta,\dot\eta)$. The density $p(\eta)$ is then obtained

$$p(\eta) = \int_{-\infty}^{\infty} p(\eta,\dot\eta)\ d\dot\eta \quad \text{where} \quad p(\eta,\dot\eta) = \frac{1}{2\pi A\omega_0}p(A). \tag{23}$$

Next the normalized noise intensity coefficient c_0 has to be identified in order to deduce ν from the estimate of ν/c_0. One way to get an estimate of c_0 is to look at the autocorrelation function $k_{\eta\eta}$. Indeed it can be shown that its envelope is exponential and that the decay rate is equal to c_0. Another way to quantify c_0 is to focus on the random process $Y = A\dot\varphi$ (see eq. (13)) which is a white noise with an intensity $\Gamma/2\omega_0^2$. Making use of the theoretical density function expression for a band-pass filtered white noise, one can also estimate c_0 and afterward deduce ν.

This is a pre-print version. Published in *International Journal of Non-Linear Mechanics* (2013) Vol. 50, p. 152-163, DOI: 10.1016/j.ijnonlinmec.2012.11.008

2.2.4. Drift and diffusion coefficients of the Fokker-Planck equation

The last method discussed in this study has been introduced in 1998 [31, 32, 33] and recently improved to account for finite sampling time effects [34, 35]. It consists in determining the states-dependent convection and diffusion coefficients of the Fokker-Planck equation describing the evolution of the transitional probability density of the random process. In the situation investigated here, it reduces to:

$$\frac{\partial}{\partial t}p(A,t+\tau|a,t) = -\frac{\partial}{\partial A}\{\mathcal{F}(A)p(A,t+\tau|a,t)\} + \frac{\Gamma}{4\omega_0^2}\frac{\partial^2}{\partial A^2}p(A,t+\tau|a,t) \tag{24}$$

Note that multiplying eq. (24) by $p(a,t)$ and integrating over a yields the evolution equation (20) of the single state probability density. This is the transport equation of the transitional probability and it features a convective component and a diffusive one. One can for example refer to [36] for the derivation of the Fokker-Planck equation with detailed explanations of the underlying assumptions. Based on the work of Kolmogorov [37], it is known that the convection and diffusion coefficients of eq. (24) are related to the 1$^{\text{st}}$ and 2$^{\text{nd}}$ transition moments:

$$\mathcal{F}(A) = \lim_{\Delta t\to 0}\frac{1}{\Delta t}\int_{-\infty}^{\infty}(a-A)\,p\,(A,t+\Delta t|a,t)\,da \tag{25}$$

$$\frac{\Gamma}{2\omega_0^2} = \lim_{\Delta t\to 0}\frac{1}{\Delta t}\int_{-\infty}^{\infty}(a-A)^2\,p\,(A,t+\Delta t|a,t)\,da. \tag{26}$$

Making use of these relationships to extract the deterministic quantities of the system has been recently proposed [31]. It is indeed possible to get from measured data the transition moments and perform numerical integrations in order to retrieve the convection and diffusion coefficients of the Fokker-Planck equation. One of the advantages of this technique is that the form of $\mathcal{F}$ does not have to be predefined to calculate the coefficients. This was not the case for the approaches presented in the previous sections or for the extended Kalman filtering technique proposed in [38]. Confronting the estimated amplitude dependent convection coefficient to the theoretical model given in eq. (19) is therefore a way to validate the assumption of the Van der Pol type deterministic behavior. It can be furthermore used to fit the deterministic growth rate, this latter being the linear contribution of the convection coefficient.

3. Experimental validation

The objective of this chapter is to validate the system identification techniques that have been presented in the previous sections. For that purpose, a well controlled experiment allowing to mimic thermoacoustic coupling in gas turbine combustion chambers is set up. More specifically, the electroacoustic feedback which is used allows to reproduce the nonlinear flame response to acoustic perturbations.

This is a pre-print version. Published in *International Journal of Non-Linear Mechanics* (2013) Vol. 50, p. 152-163, DOI: 10.1016/j.ijnonlinmec.2012.11.008

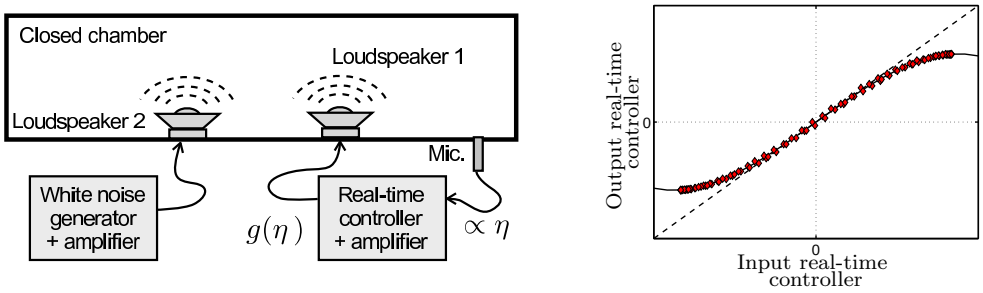

Figure 2: Left: Sketch of the experimental set-up. The electro-acoustic feedback which can be adjusted to yield self-induced acoustic oscillations in the chamber involves the microphone, the real-time controller, an amplifier and loudspeaker 1. The additive stochastic forcing is produced with loudspeaker 2. Right: Input-Output command $g(x) = c_3 x - c_4 x^3$ (solid line) with superimposed experimental data (bullets).

3.1. Experimental set-up

An electro-acoustic Van der Pol oscillator has been developed to validate the identification techniques. A sketch of the set-up is presented in figure 2. Its main components are a closed tube containing two loudspeakers fed by amplified signals, a microphone and a real time controller. The microphone signal is routed to the first loudspeaker via the real time controller. Input/Output analog modules are connected to this latter controller which includes a reconfigurable field programmable gate array (FPGA). This set-up allows accurate arithmetic transformations of the input signal at a rate which is 3 order of magnitude faster than the acoustic eigenfrequency considered. The purpose of this set-up is to generate self-induced acoustic oscillations with Van der Pol type dynamics. Without feedback control, i.e. when the microphone is disconnected, the amplitude of each of the eigenmodes of the enclosure can be approximated by the following second order differential equation

$$\ddot{\eta} + \alpha\dot{\eta} + \omega_0^2\eta = 0, \tag{27}$$

where ω_0 and α are the eigenfrequency and the natural damping coefficient of the eigenmode. The damping coefficient includes acoustic energy absorption in the volume and on the boundaries.
With the loudspeaker which behaves as an acoustic volume source, one can write the differential equation governing the modal amplitude η as follows

$$\ddot{\eta} + \alpha\dot{\eta} + \omega_0^2\eta = c_1\dot{v}, \tag{28}$$

where v is the input signal feeding the loudspeaker and c_1 accounts for both the electroacoustical conversion factor of the loudspeaker and its position with respect to the acoustic eigenmode considered. One can write $v = g(c_2 p)$ where g is the input-output relationship defined in the real-time controller, p is the acoustic pressure measured by the microphone and c_2 depends on its

This is a pre-print version. Published in *International Journal of Non-Linear Mechanics* (2013) Vol. 50, p. 152-163, DOI: 10.1016/j.ijnonlinmec.2012.11.008

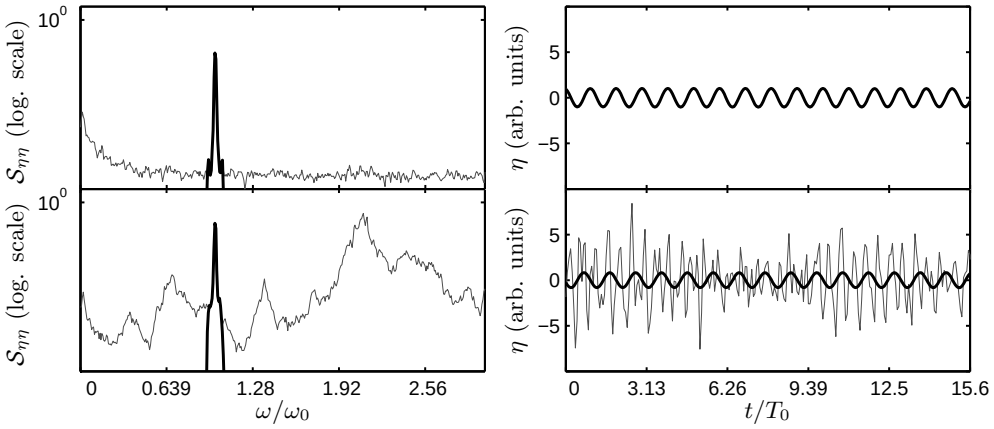

Figure 3: Limit cycle oscillation obtained from the electroacoustic Van der Pol oscillator. The acoustic pressure spectrum and time trace are respectively plotted on the left and right sides (acoustic pressure signal recorded with the microphone). The thick solid lines correspond to the signal filtered on a narrow bandwidth around the self-excited eigenmode peak. *Upper diagrams:* Loudspeaker 2 is switched off. *Lower diagrams:* Loudspeaker 2 provides the additive stochastic noise to the system.

sensitivity. It yields $v = g(c_2\psi(\mathbf{x}_{\rm mic})\eta(t))$. If the function g is defined as $g(x) = c_3x - c_4x^3$ with its corresponding time derivative $c_3\dot{x} - 3c_4\dot{x}x^2$, one can write

$$\ddot{\eta} + \omega_0^2\eta = \dot{\eta}(\beta - \alpha - \kappa\eta^2), \tag{29}$$

where $\beta = c_1c_2c_3\psi_{\rm mic}$ and $\kappa = 3c_1c_2^3c_4\psi_{\rm mic}^3$ which is the equation for the Van der Pol oscillator. The input-output command defined in the FPGA is shown in figure 2 together with experimental data. The user interface used to define the real-time transformation has been built such that the parameters c_3 and c_4, and therefore β and κ, can be modified on-line. This allows to instantaneously change from a linearly stable to a linearly unstable situation ($\alpha > \beta$ and $\alpha < \beta$ respectively). Note that the third order nonlinearity imposed by the controller allows to mimic the flame response saturation. It must be mentioned that an analog band-pass filter is plugged between the microphone and the real-time controller. This filter is used to select one particular mode of the chamber for the electroacoustic feedback.

When the parameters are set such that $\beta > \alpha$, the electro-acoustic Van der Pol evolves to a limit cycle. In practical combustion system prone to thermo-acoustic coupling, the limit cycles are perturbed by the background noise produced by the highly turbulent reactive flow. It is generally valid in practice to assume that the additive noise component dominates the multiplicative one, the latter being induced by temperature fluctuations in the combustion chamber (e.g. [39] for the particular case of a cryogenic flames used for rocket engine). In the experimental setup presented here, the turbulence-induced noise is mimicked using a second loudspeaker fed with a white noise generator. When the second loudspeaker is working, the system dynamics can be approximated

This is a pre-print version. Published in *International Journal of Non-Linear Mechanics* (2013) Vol. 50, p. 152-163, DOI: 10.1016/j.ijnonlinmec.2012.11.008

by the stochastic Van der Pol equation:

$$\ddot{\eta} + \omega_0^2 \eta = \dot{\eta}(\beta - \alpha - \kappa\eta^2) + \xi, \tag{30}$$

In figure 3, a typical limit cycling state with and without stochastic forcing is presented. One can see that when the second loudspeaker is acting several eigenmodes of the chamber are visible in the spectrum which is not the case when stochastic forcing is not applied. In particular, at approximately twice the frequency of the main peak one can see that the response to the stochastic forcing is important. This is due to the location of the loudspeaker 2 which favors the amplification of the eigenmodes corresponding to this frequency range.

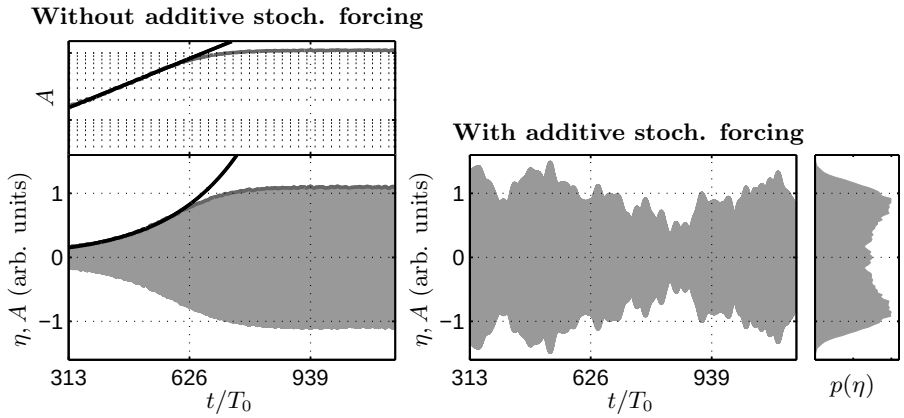

Figure 4: Linearly unstable electroacoustic Van der Pol oscillator (same conditions as for figure 3). When the feedback loop is activated, the system evolves into a limit cycling state. *Left:* The linear growth rate $\nu = (\beta - \alpha)/2$ can be directly measured by fitting a line on the logarithmic plot of the acoustic amplitude extracted from the noise-free transient (Loudspeaker 2 is switched off). *Right:* Loudspeaker 2 is switched on i.e. additive stochastic forcing is applied. A snapshot of the filtered acoustic pressure signal is presented (the filter bandwidth is shown in figure 3). The distribution of the filtered acoustic pressure is given on the right.

From the time traces presented in figure 3, it might be wrongly concluded that the stochastic forcing does not affect the acoustic oscillations associated to the main peak (see filtered signal plotted as a bold solid line). One will later see that the amplitude dynamics is much slower than the acoustic oscillations, cannot be seen from such short period of time but is actually impacted by the stochastic forcing imposed by Loudspeaker 2.

Beyond its simplicity, the main advantage of this experimental setup is that on the one hand the "deterministic" quantities can be directly obtained using the noise-free system (Loudspeaker 2 turned off) and on the other the different theoretical approaches presented in the previous section can be used to estimate these quantities from stochastically perturbed limit cycle data (Loudspeaker 2 turned on). This is illustrated in figures 4 and 5.

In figure 4, the operating conditions are the same as the ones used in figure 3. By changing

This is a pre-print version. Published in *International Journal of Non-Linear Mechanics* (2013) Vol. 50, p. 152-163, DOI: 10.1016/j.ijnonlinmec.2012.11.008

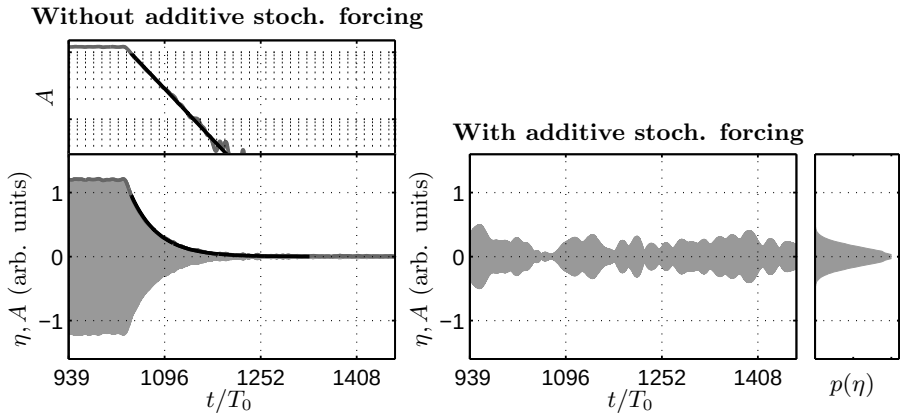

Figure 5: Linearly stable electroacoustic Van der Pol oscillator. When the gain is changed such that β becomes smaller than α, the system evolves to the equilibrium. *Left:* The linear damping rate $\nu = (\beta - \alpha)/2$ can be directly measured by fitting a line on the logarithmic plot of the acoustic amplitude A extracted from the noise-free transient (Loudspeaker 2 is switched off). *Right:* Loudspeaker 2 is switched on i.e. additive stochastic forcing is applied. A snapshot of the filtered acoustic pressure signal is presented (the filter bandwidth is the same as in figure 3). The distribution of the filtered acoustic pressure is given on the right.

the value of the coefficient c_3 of the real-time controller, the system which was linearly stable ($\alpha > \beta$) becomes unstable ($\alpha < \beta$). The acoustic oscillations start growing at the exponential rate $(\beta - \alpha)/2$. This growth rate can be directly measured by fitting a line on the logarithmic plot of the acoustic pressure amplitude which is obtained by taking the absolute value of the Hilbert transform of the raw signal. When the amplitude reaches a certain level, the effects of the cubic nonlinearity imposed by the real time controller become visible. The oscillation amplitude growth deviates from the exponential curve and the system finally stabilizes on a limit cycle. The limit cycle amplitude A_0 can be used to estimate the nonlinearity coefficient κ since $\kappa = 8\nu/A_0^2$.

In figure 5 on the left side, one can see that when the value of c_3 is suddenly changed, the system which was initially stabilized on a limit cycle becomes linearly stable and the oscillation amplitude exponentially decreases to the equilibrium which is now the attractor. In the same way as for the growth rate, the damping rate is obtained by fitting a line on the logarithmic plot of the amplitude decay.

The diagrams on the right in figure 4 and 5 are now considered. The stable limit cycle and the asymptotically stable origin respectively obtained in the last mentioned figures for two values of c_3, one yielding $\beta > \alpha$ and the other $\beta < \alpha$ are now perturbed with a stochastic forcing produced by means of the second loudspeaker. Time traces of the corresponding filtered signals are presented together with the distribution of the acoustic pressure filtered around the peak. The short time trace ($\approx$ 15 cycles) plotted as a bold black solid line in the lower right diagram of figure 3 was extracted from the same filtered data set as the one given in gray in figure 4 on the right. The width

This is a pre-print version. Published in *International Journal of Non-Linear Mechanics* (2013) Vol. 50, p. 152-163, DOI: 10.1016/j.ijnonlinmec.2012.11.008

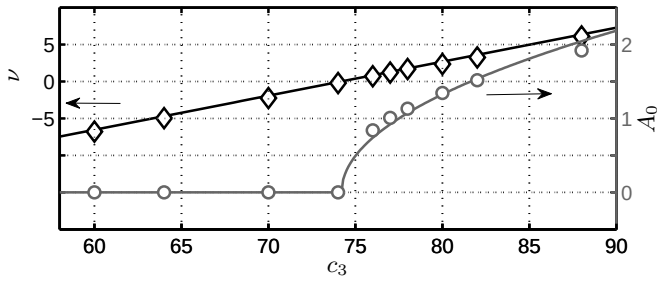

Figure 6: Bifurcation diagram of the noise-free electroacoustic Van der Pol oscillator. Solid lines have been fitted on the experimental data.

of the band-pass filter which has been applied is approximately one tenth of the eigenfrequency considered (see the lower left diagram in figure 3), which is sufficient to capture the main dynamics associated with the stochastically perturbed limit cycle. It is important to note that from this longer snapshot (≈ 850 cycles), the influence of the stochastic forcing on the limit cycle amplitude is clearly visible which is not the case if one considers only 15 consecutive cycles as shown in the lower right diagram of figure 3. This is because the acoustic amplitude is a random process having a much longer correlation time than the acoustic period, and this is related to the fact that the right hand side in eq. (30) is small compared to the terms in the left hand side.
In the diagrams on the right in figure 4 and 5, the noise intensity Γ is set to the same level. A bimodal density function is obtained for the case $\beta > \alpha$ while a gaussian like distribution characterizes the stochastically perturbed asymptotically stable origin ($\beta < \alpha$). One can refer to the work of [40] for a detailed analysis of the distribution shape transition at the Hopf bifurcation. The different methods presented in the previous section are tested with the recorded data sets and the estimates for the growth rate ν and the nonlinearity κ can be compared to the values obtained with the direct method which is applied to the noise-free system.

3.2. Deterministic behavior

The noise-free electroacoustic Van der Pol oscillator was investigated in the vicinity of its Hopf bifurcation by varying the parameter c_3, resulting in a variation of β while all the other parameters (α, κ, ω_0) remain constant. The resulting bifurcation diagram is given in figure 6. The growth/damping rates for each value of c_3 were extracted as explained above and the linear dependance of ν with respect to c_3 is confirmed.

3.3. Stochastic forcing and growth rate extraction

The different methods presented to estimate deterministic parameters ν_e, κ_e and Γ_e from stochastically perturbed limit cycles are now applied to experimental data. One has to mention that the value of c_4 – therefore the nonlinearity coefficient κ – was kept constant for all the measurements. The noise intensity was also kept constant for all the conditions. While the measurement of the

This is a pre-print version. Published in *International Journal of Non-Linear Mechanics* (2013) Vol. 50, p. 152-163, DOI: 10.1016/j.ijnonlinmec.2012.11.008

deterministic values for ν and κ is possible using the noise-free setup, the noise intensity can only be deduced from the stochastic based approaches. Since it has been kept constant for all the measurements, the theoretical value has been deduced by averaging the entire set of estimates. It will be shown that the standard deviation of this set of estimates for Γ is much lower than the estimate mean. For each of the methods which were applied to acoustic pressure records containing approximately 40 000 cycles, theoretical models calculated using the deterministic values for ν, κ and Γ are superimposed to the corresponding experimental data.

When the system is asymptotically stable, it is possible to extract the damping rate by fitting the power spectral density of the pressure signal with a second order model given in equation (15). This approach was applied to acoustic pressure signals obtained from the stochastic electroacoustic Van der Pol oscillator for values of c_3 low enough such that $\nu < 0$. Two examples are given in figure 7a where the experimental power spectral densities (PSD) are superimposed to the theoretical ones. It has been mentioned that this method works when ν is negative. Another condition which must be satisfied to apply this method is the following: the noise intensity must be low enough so that the effect of the cubic nonlinearity of the feedback is negligible.

For the case of linearly unstable system, it has been shown in the previous section that a strategy based on the linearization of the amplitude equation can be adopted. In this situation, the inverse of the growth rate is approximately twice the time constant of the amplitude equation (16). This exponential decay constant characterizes the time taken by the system to recover its limit cycle amplitude when it has been perturbed. Making use of this information, it is possible to compute the PSD of the limit cycle amplitude fluctuations and estimate its cut-off frequency to retrieve the growth rate. Examples are shown in figure 7b where experimental PSD are plotted together with the theoretical ones. Note that the amplitude fluctuations induced by the white noise perturbation must be small compared to the deterministic limit cycle amplitude to justify the linearization and apply this technique successfully.

Another approach based on the solution of the Fokker-Planck equation associated to the amplitude and phase random processes can be used. The extraction of the deterministic quantities is performed in two steps: Firstly the deterministic limit cycle amplitude A_0 and the ratio ν/c_0 are estimated by fitting the density function of the random amplitude process, or alternatively the one of η, with the theoretical models given in eqs. (22) and (23) respectively. This is exemplified in Figs. 7c. Secondly the normalized noise intensity c_0 is obtained by estimating the variance of the theoretically gaussian density function of the random process $A\dot{\varphi}$ as shown in Fig. 7d. Together with the estimation of ν/c_0, it is possible to deduce ν. One can see in figures 7c and 7d that the distribution obtained from the stochastically perturbed limit cycles closely follow the ones from the theoretical model. Note that in contrast with the linearization method presented in the previous paragraph, the assumption $A' \ll A_0$ is not required to derive the equations. However, as the ratio ν/c_0 tends to zero, the estimation of the deterministic limit cycle amplitude from the Rayleigh-like distribution is less and less accurate, which in turns decrease the quality of the estimate of ν.

In Fig. 7c, one can see that when the growth rate is increased the PDF follows the same kind of

This is a pre-print version. Published in *International Journal of Non-Linear Mechanics* (2013) Vol. 50, p. 152-163, DOI: 10.1016/j.ijnonlinmec.2012.11.008

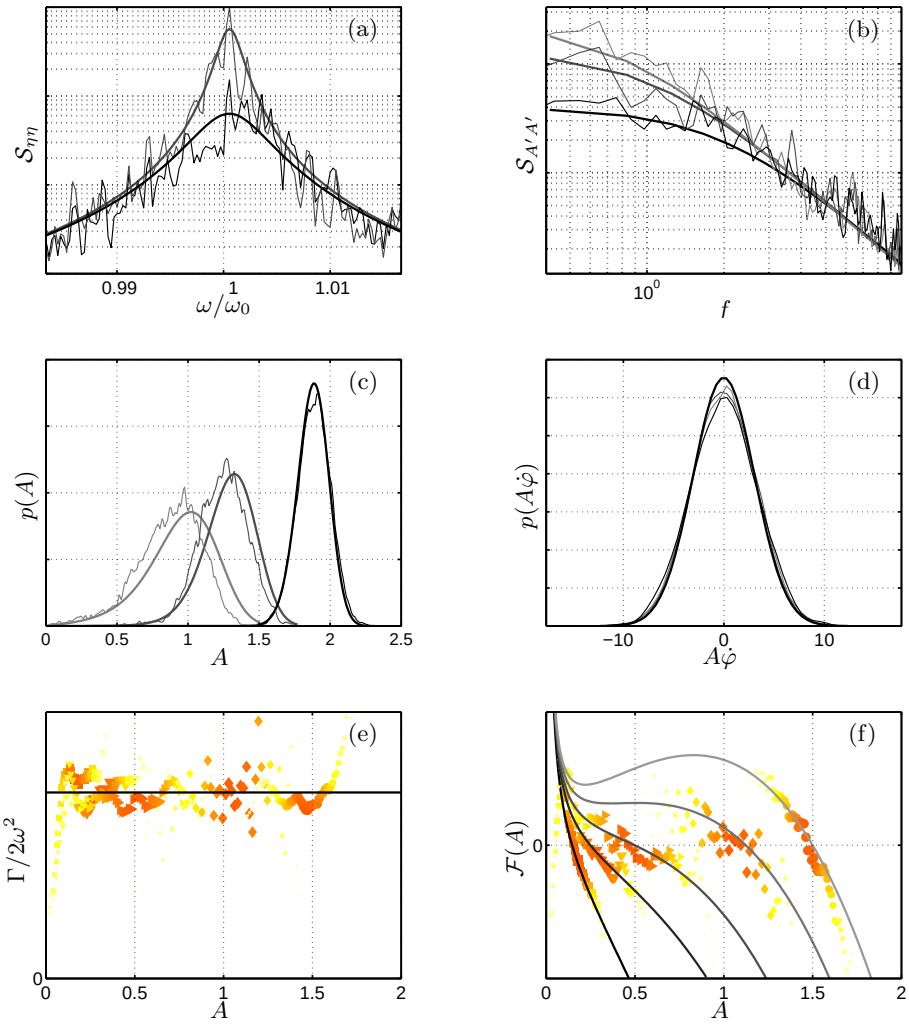

Figure 7: Comparisons between numerical applications of the theoretical models using the deterministic parameters obtained from the noise-free system (thick lines) and experimental data (thin lines or symbols). (a) Linearly stable cases: $\nu < 0$. Theoretical curves from eq. (15). The damping rate ν is decreased as the curves darken. (b) PSD of the limit cycle amplitude fluctuations given from eq. (17). The growth rate ν is increased as the curves darken. (c) PDF of the amplitude process. The theoretical curves are calculated using eq. (22) (the larger the growth rate, the darkener the curve). (d) PDF the process $A\dot{\varphi}$. (e) and (f) Second and first transition moments of the amplitude process. The theoretical curve for the first moment is computed using eq. (19). Linearly stable and unstable cases (resp. $\nu < 0$ and $\nu > 0$) are presented (the larger ν the brightener the curve). The symbols are colored as function of $p(A)$.

This is a pre-print version. Published in *International Journal of Non-Linear Mechanics* (2013) Vol. 50, p. 152-163, DOI: 10.1016/j.ijnonlinmec.2012.11.008

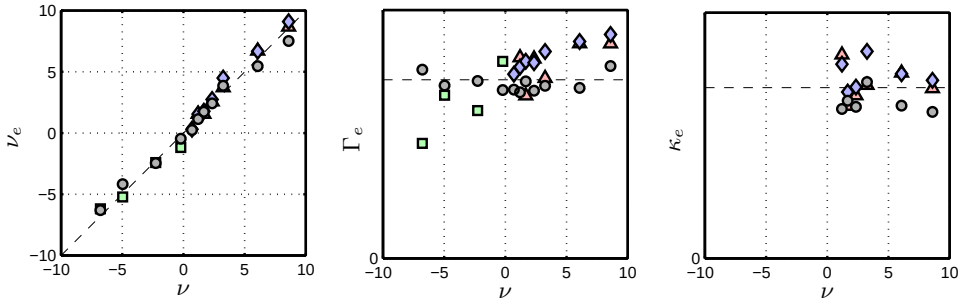

Figure 8: Overview of the estimation of the deterministic components. Squares: method based on the PSD of the pressure signal. Triangles: method based on the PSD of the eigenmode amplitude. Diamonds: method based on the solutions of the Fokker-Planck equation associated to the amplitude process. Circles: method based on the estimation of the Fokker-Planck equation coefficients.

behavior as the Rice distribution with a transition from a Rayleigh-like density to a Gaussian-like one centered on A_0. Note that the amplitude term in the exponent in eq. (22) is quartic and not quadratic as for the Rice distribution.

The last approach is more general and can be equally applied to linearly stable and unstable oscillators – i.e. ν being negative or positive – which was not the case for the previous estimation methods. It has been shown that the convection and diffusion coefficients of the Fokker-Planck equation associated to the amplitude equation – which are the related to the deterministic and stochastic parameters of the system – can be estimated through the first and second transition moments respectively. The method is applied to different time traces recorded at various growth rates. The results are shown in Fig. 7e and 7f. It is shown that the estimated transition moments for a series of growth/damping rates match the ones deduced from the noise-free system measurements with a remarkable agreement. Note that although the process η, standing for the acoustic eigenmode amplitude, can generally be assumed to be Markovian as shown in the previous section, it is usually difficult in real applications to calculate accurate transition moments for this process because of sampling rate limitations. Applying this method to the process η itself would be theoretically feasible but would give in practice poor quality estimates of the deterministic quantities. Looking at the corresponding amplitude process A, which is also Markovian and which features a much slower deterministic dynamics is therefore a good measure to compensate the coarseness of the recorded data set.

An overview of the estimated values for ν, Γ and κ is finally presented in figure 8. It was shown that the strategy consisting in estimating the transition moments of the amplitude process is the most general and provide good estimates of the deterministic quantities. However, the duration of the signal, its sampling rate and the delay used in the moments calculation affect the statistics quality as already shown in [33] for the case of a Pitchfork bifurcation. It is therefore interesting to compare the results obtained with the general method to the ones obtained with the other

This is a pre-print version. Published in *International Journal of Non-Linear Mechanics* (2013) Vol. 50, p. 152-163, DOI: 10.1016/j.ijnonlinmec.2012.11.008

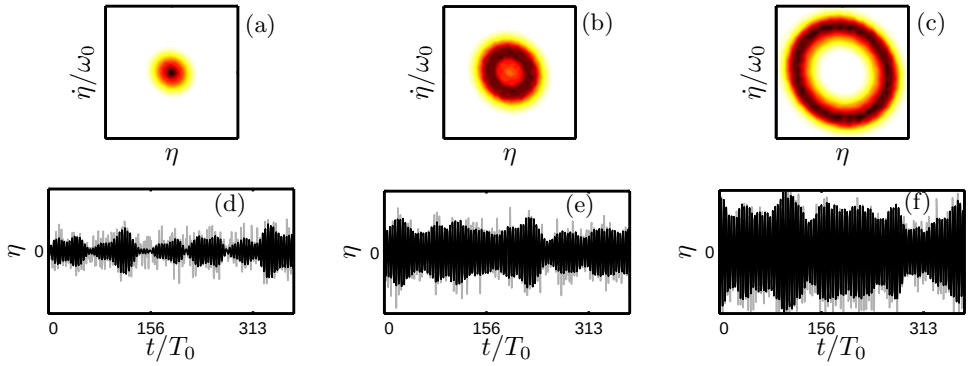

Figure 9: Acoustic pressure signals corresponding to 3 different operating conditions (single parameter variation). (d) to (f): snapshots of the recorded time traces. The black lines stand for the filtered signal. The band-pass filter which was used is centered around the dominant peak at ω_0. The bandwidth was defined as $\Delta\omega = 0.3\,\omega_0$. (a) to (c): corresponding joint PDF computed from the filtered pressure signal which is proportional to η.

approaches in order to get more confidence in the deterministic parameters estimation.

4. Application to engine data

The different extraction methods are now applied to dynamic pressure signals recorded in a gas turbine combustion chamber. Three different operating conditions have been analyzed, the second and the last one being out of the nominal operation range. The time traces are presented in figure 9 with the corresponding probability density functions of the joint response process $(\eta, \dot{\eta}/\omega_0)$, where η is proportional to the acoustic pressure in the combustor band-pass filtered around the dominant peak. The joint probability density function is a good indicator of the system stability, with gaussian-like and ring shaped densities for stable and unstable cases respectively.
The growth rate estimation was done using the different methods. For the stable case (figure 9d), a close-up view on the power spectral density of the signal with its best fit using eq. (15) is shown in figure 10a. An estimate of the damping rate is obtained from this fit.
The power spectral density of the fluctuating amplitude for the strongest limit cycle (figure 9f) is presented in figure 10b with the best fitted first order low pass filter, which directly give access to a growth rate estimate. Note that this strategy does not apply when the normalized noise intensity is to high with respect to the growth rate which is for example the case for the intermediate operating condition shown in 9e. The method based on the solutions of the Fokker-Planck equation associated to the amplitude response process was used for the two cases where the system operates on a stochastically perturbed limit cycle (see figure 9e and 9f) and the results are shown in figure 10c. Finally, the strategy consisting in fitting the post-processed first transition moment of the amplitude process is presented in figure 10d. This method, which is the most general, can be applied to each of the cases presented in figure 9. One can see that the theoretical curves closely follow the amplitude dependent transition moment.

This is a pre-print version. Published in *International Journal of Non-Linear Mechanics* (2013) Vol. 50, p. 152-163, DOI: 10.1016/j.ijnonlinmec.2012.11.008

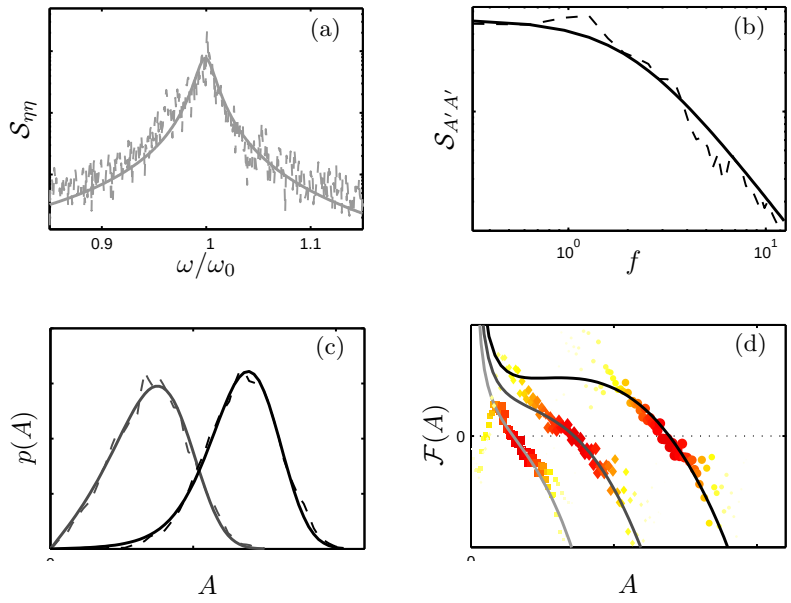

Figure 10: Post-processed acoustic pressure data (dashed lines and symbols) plotted together with the corresponding best fits using theoretical models. (a) Linearly stable operating condition (diagrams (a) and (d) in figure 9). The PSD of the acoustic pressure was fitted using eq. (15). (b) Linearly unstable condition (diagrams (c) and (f) in figure 9). PSD of the limit cycle amplitude fluctuations is fitted using eq. (17). (c) Linearly unstable conditions (diagrams (b)-(e) and (c)-(f) in figure 9 for gray and black curves respectively). The PDF of the amplitude process were fitted using eq. (22). (d) First transition moment of the amplitude process for the three operating conditions (a), (b) and (c) shown in figure 9. The theoretical curve is fitted using eq. (19).

The growth rate estimates for the three operating conditions analyzed are presented in table 1, where the application range of the different approaches is highlighted. It can be concluded that all the estimates are in very good agreement.

5. Conclusion

Different strategies are proposed to identify deterministic quantities governing stochastically perturbed thermoacoustic limit cycles. In gas turbine applications, the knowledge of these parameters is crucial to properly design damping equipment. It is shown that the identification can be achieved by considering either the linearized version of the equation governing the limit cycle amplitude or the solutions of the associated Fokker-Planck equation or its convection and diffusion coefficients. The possibility to extract these deterministic quantities using several methods brings a high level of confidence in the estimates that are obtained. In a first step, the different approaches are applied to experimental data obtained using a well controlled electro-acoustic Van der Pol oscillator. This is done to demonstrate the accuracy of the growth rate estimates in practical conditions involving linearly unstable acoustic system, featuring a plurality of eigenmodes, a realistic random excitation and a non-linear feedback response used to mimic the nonlinear dynamic behavior of the flame. In

This is a pre-print version. Published in *International Journal of Non-Linear Mechanics* (2013) Vol. 50, p. 152-163, DOI: 10.1016/j.ijnonlinmec.2012.11.008

	Approach 1 Fig. 10a	Approach 2 Fig. 10b	Approach 3 Fig. 10c	Approach 4 Fig. 10d
case 1, Fig. 9d	-4.5	-	-	-4.2
case 2, Fig. 9e	-	-	2	2.2
case 3, Fig. 9f	-	6.2	6.1	5.9

Table 1: Estimates of the growth rate ν for the three conditions presented in figure 9 using the different theoretical approaches (see figure 10).

the last section, the theoretical framework presented and validated in the first part is successfully applied to pulsation data recorded in gas turbine combustion chamber. To the authors' knowledge it is the first time that combustion instabilities growth rates and nonlinearity coefficients are quantitatively measured on practical system.

References

[1] T. C. Lieuwen, V. Yang, Combustion instabilities in gas turbines, operational experience, fundamental mechanisms, and modeling, American Institute of aeronautics and astronautics, Inc., 2005.

[2] R. Balachandran, B. O. Ayoola, C. F. Kaminski, A. P. Dowling, E. Mastorakos, Experimental investigation of the nonlinear response of turbulent premixed flames to imposed inlet velocity oscillations, Combust. & Flame 143 (2005) 37–55.

[3] N. Noiray, D. Durox, T. Schuller, S. Candel, A unified framework for nonlinear combustion instability analysis based on the flame describing function, Journal of Fluid Mechanics 615 (2008) 139–167.

[4] K. Kim, J. Lee, B. Quay, D. Santavicca, Spatially distributed flame transfer functions for predicting combustion dynamics in lean premixed gas turbine combustors, Combustion and Flame 157 (9) (2010) 1718–1730.

[5] S. Schimek, J. Moeck, C. Paschereit, An experimental investigation of the nonlinear response of an atmospheric swirl-stabilized premixed flame, Journal of Engineering for Gas Turbines and Power 133 (10).

[6] P. Palies, D. Durox, T. Schuller, S. Candel, Nonlinear combustion instability analysis based on the flame describing function applied to turbulent premixed swirling flames, Combustion and Flame 158 (10) (2011) 1980–1991.

[7] S. Nagaraja, K. Kedia, R. Sujith, Characterizing energy growth during combustion instabilities: Singularvalues or eigenvalues?, Proc. Combust. Inst. 32 (2009) 2933–2940.

[8] K. Wieczorek, C. Sensiau, W. Polifke, F. Nicoud, Assessing non-normal effects in thermoacoustic systems with mean flow, Physics of Fluids 23 (10).

[9] N. Noiray, B. Schuermans, Theoretical and experimental investigations on damper performance for suppression of thermoacoustic oscillations, Journal of sound and vibration, 331 (2012) 2753–2763.

[10] T. Poinsot, B. Yip, D. Veynante, A. Trouve, J. M. Samaniengo, S. Candel, Active control - an investigation method for combustion instabilities, Journal de physique III 2 (7) (1992) 1331–1357.

[11] D. Harrje, F. Reardon, Liquid propellant rocket instability, Tech. rep., NASA SP-194 (1972).

This is a pre-print version. Published in *International Journal of Non-Linear Mechanics* (2013) Vol. 50, p. 152-163, DOI: 10.1016/j.ijnonlinmec.2012.11.008

[12] T. Lieuwen, Online combustor stability margin assessment using dynamic pressure data, Journal of Engineering for Gas Turbines and Power, ASME Trans. 127 (2005) 478–482.
[13] T. Yi, E. J. Gutmark, Online prediction of the onset of combustion instability based on the computation of damping ratios, J. Sound and Vib. 310 (2008) 442–447.
[14] F. E. C. Culick, Unsteady motions in combustion chambers for propulsion systems, AGARDograph, NATO/RTO-AG-AVT-039, 2006.
[15] P. Clavin, J. S. Kim, F. A. Williams, Turbulence-induced noise effects on high-frequency combustion instabilities, Combust. Sci. Tech. 96 (1994) 61–84.
[16] T. C. Lieuwen, Statistical characteristics of pressure oscillations in a premixed combustor, J. Sound Vib. 260 (2003) 3–17.
[17] T. Lieuwen, A. Banaszuk, Background noise effects on combustor stability, J. Propuls Power 21 (1) (2005) 25–31.
[18] I. C. Waugh, M. Geuss, M. P. Juniper, Triggering, bypass transition and the effect of noise on a linearly stable thermoacoustic system, Proc. Combust. Inst. 33 (2011) 2945–2952.
[19] R. C. Stratonovich, Topics in the theory of random noise, Vol. 2, Gordon & Breach, New-York, 1963.
[20] P.-T. D. Spanos, Stochastic analysis of oscillators with non-linear damping, Int. J. Non-linear Mechanics 13 (1978) 249–259.
[21] J. B. Roberts, P. D. Spanos, Invited review no. 1: Stochastic averaging: an approximate method of solving random vibration problems, Int. J. Non-linear Mechanics 21 (2) (1986) 111–134.
[22] S. Evesque, A. P. Dowling, A. M. Annaswamy, Self-tuning regulators for combustion oscillations, Proc. R. Soc. Lond. A 459 (2003) 1709–1749.
[23] T. Sattelmayer, Influence of the combustor aerodynamics on combustion instabilities from equivalence ratio fluctuations, Journal of Engineering for Gas Turbines and Power, ASME Trans. 125 (2003) 11–19.
[24] W. Polifke, C. Lawn, On the low-frequency limit of ame transfer functions, Combust. & Flame 151 (2007) 437–451.
[25] J. Moeck, M. Bothien, S. S., A. Lacarelle, C. O. Paschereit, Subcritical thermoacoustic instabilites in a premixed combustor, in: AIAA paper 2008-2946 , 14^{th} Aeroacoustics Conference (29th AIAA Aeroacoustics Conference), Vancouver, British Columbia Canada, 2008.
[26] P. Clavin, E. Siggia, Turbulent premixed flames and sound generation, Combust. Sci. Technol. 78 (1991) 147–155.
[27] C. Hirsch, J. Wäsle, A. Winkler, T. Sattelmayer, A spectral model for the sound pressure from turbulent premixed combustion, Proc. Combust. Inst. 31 (2007) 1435–1441.
[28] R. Rajaram, T. Lieuwen, Acoustic radiation from turbulent premixed flames, J. Fluid Mech. 637 (2009) 357–385.
[29] N. Krylov, N. Bogoliubov, Introduction to nonlinear mechanics, Princeton University Press, 1949.
[30] W.-Q. Zhu, J.-S. Yu, On the response of the van der pol oscillator to white noise excitation, J. Sound & Vib. 117 (3) (1987) 421–431.
[31] S. Siegert, R. Friedrich, J. Peinke, Analysis of data sets of stochastic systems, Physics Letters A 243 (1998) 275–280.
[32] R. Friedrich, S. Siegert, J. Peinke, S. Lück, M. Siefert, M. Lindemann, J. Raethjen, G. Deuschl, G. Pfister, Extracting model equations from experimental data, Physics Letters A 271 (2000) 217–222.
[33] J. Gradisek, S. Siegert, R. Friedrich, I. Grabec, Analysis of time series from stochastic pro-

This is a pre-print version. Published in *International Journal of Non-Linear Mechanics* (2013) Vol. 50, p. 152-163, DOI: 10.1016/j.ijnonlinmec.2012.11.008

cesses, Physical Review E 62 (3146–3155) (2000) 217–222.
[34] S. J. Lade, Finite sampling interval effects in kramers-moyal analysis, Physics Letters A 373 (2009) 3705–3709.
[35] C. Honisch, R. Friedrich, Estimation of kramers-moyal coefficients at low sampling rates, Phys. Rev. E 83 (6) (2011) 066701.
[36] M. Scott, Applied stochastic processes, *http://www.math.uwaterloo.ca/∼mscott/Notes.pdf*, 2011.
[37] A. N. Kolmogorov, Über die analytischen methoden in der wahrscheinlichkeitsrechnung, Math. Ann. 140 (1931) 415–458.
[38] A. Sitz, U. Schwarz, J. Kurths, H. U. Voss, Estimation of parameters and unobserved components for nonlinear systems from noisy time series, Phys. Rev. E 66 (2002) 016210.
[39] F. Richecoeur, S. Ducruix, P. Scouflaire, S. Candel, Effect of temperature fluctuations on high frequency acoustic coupling, Proc. Combust. Inst. 32 (2009) 1663–1670.
[40] A. Juel, A. G. Darbyshire, T. Mullin, The effect of noise on pitchfork and hopf bifurcations, Proc. R. Soc. Lond. A 453 (1997) 2627–2647.

Appendix

This does not exclude the possibility of so–called non–normal growth of the energy of the system for instance discussed in e.g. [7] or [18]. This is because the norm of the state vector in eq. (2) does *not* represent the energy of the system. In order to analyze the internal energy of the system, one can always augment the system an additional output vector $\boldsymbol{\eta}_e$ and matrix $\mathbf{C_e}$ such that the norm of $\boldsymbol{\eta}_e$ represents the internal energy of the system. However, instead of examining $||e^{\mathbf{A}\,t}||$ one would have to examine $||\mathbf{C_e}\,e^{\mathbf{A}\,t}||$ to find the bounds of the energy. Analogous to [7] the initial state vector that maximizes the transient energy can be obtained by a singular value decomposition. A question that is not addressed in that reference is: "Is it possible to bring the system in this worst-case state?". This question can be answered by first making sure that all the physical inputs to the system are correctly captured in the matrix B. Note that initial conditions can always be modeled as additional inputs, so, without loss of generality one can analyze a system $||\mathbf{C_e}\,e^{\mathbf{A}\,t}\,\mathbf{B_e}||$ with zero initial conditions. The answer to the question is then given by the controllability of the system, which is given by the Gramian of $\mathbf{A}$ and $\mathbf{B_e}$.

This is a pre-print version. Published in *International Journal of Non-Linear Mechanics* (2013) Vol. 50, p. 152-163, DOI: 10.1016/j.ijnonlinmec.2012.11.008